Architecture-Driven Porous Copper Nanofiber Networks for High-Rate CO_2 Electrochemical Reduction to Ethylene

Abdelrahman M. Abdelmohsen[1], Abdelrahman A. Ashour [1], Ghada E. Khedr[2], Ahmed Aboueloyoun Taha[1], Hossam N. Akl[1], and Nageh K. Allam[1, *]

[1]Energy Materials Laboratory, Physics Department, School of Sciences and Engineering, The American University in Cairo, New Cairo 11835, Egypt.

[2]Department of Analysis and Evaluation, Egyptian Petroleum Research Institute, Cairo, 11727, Egypt

*** Corresponding Author's email: nageh.allam@aucegypt.edu**

Contents

1 SI-1 Experimental section

1.1 Materials

1.2 Electrochemical measurements

1.3 Material Characterization.

1.4 Calculation

2 SI-2 Figures and Tables

Figure S1. Photographs of the four precursor syringes containing Cu acetate/PVP solutions at different Cu loadings (3.5%, 7%, 14%, and 28%).

Figure S2. SEM images of the gas diffusion layer (GDL) before catalyst deposition.

Figure S3. Schematic of Cu-nanofiber GDE fabrication: solution preparation, electrospinning, calcination to Cu NFs, ink preparation, and GDE fabrication.

Figure S4. Schematic illustration of the flow electrolyzer cell.

Figure S5. Image of the experimental setup for the electrochemical CO_2 reduction reaction (CO_2RR).

Figure S6. SEM pictures of Cu/PVP nanofibers at Cu concentrations of (a) 3.5%, (b) 7%, (c) 14%, and (d) 28%. The top row (1 μm): entire fiber morphology and network structure. Bottom row (500 nm).

Figure S7. SEM pictures of calcined Cu/PVP samples on the GDL (a) 3.5%, (b) 7%, (c) 14%, and (d) 28%. Top row (1 μm): comprehensive morphology of the calcined structures on the gas diffusion layer (GDL); Bottom row (500 nm).

Figure S8. EDX measurements of all Cu/PVP fibers before calcination. (a) Cu/PVP 3.5%, (b) Cu/PVP 7%, (c) Cu/PVP 14%, (d) Cu/PVP 28%.

Table S1. Elemental composition of all Cu/PVP fibers before calcination, as revealed from the EDX analysis.

Figure S9. EDX measurements of all Cu/PVP powder after calcination. (a) Cu/PVP 3.5%, (b) Cu/PVP 7%, (c) Cu/PVP 14%, (d) Cu/PVP 28%.

Table S2. Elemental composition of all Cu/PVP powder after calcination, as revealed from the EDX analysis.

Figure S10. The N_2 adsorption/desorption isotherms and BJH pore size distribution for Cu/PVP 3.5%, 14%, and 28%.

Figure S11. TEM image and corresponding EDS elemental mapping of the Cu/PVP 28% composite.

Figure S12. XPS of the Cu 2p for all Cu/PVP nanofiber samples.

Figure S13. GC spectra of Cu/PVP 7% (a) at 500 mA/cm^2 (b) at 700 mA/cm^2.

Table S3. Comparison of the FE of ethylene with the most relevant literature.

Figure S14. ECSA measurements of the Cu/PVP samples. (a, b, c, d), Cyclic voltammetry profiles were obtained for the 3.5%, 7%,14% and 28% samples at sweep rates of 10, 20, 30, 40, 50, 60, 70, 80, 90, 100, 110, and 120 mV/s, respectively.

Figure S15. CV at different scan rates and ECSA measurements of the Cu/PVP 7% after short-term CO_2RR operation.

Figure S16. (a) Nyquist plots obtained from EIS measurements. **(b)** Distribution of relaxation times (DRT) spectra of the Cu/PVP 7% after short-term CO_2RR operation.

Figure S17. SEM images of Cu/PVP 7% after stability measurement at current densities of **(a)** 400 mA, **(b)** 500 mA, and **(c)** 600 mA.

Table S4. Calculated Gibbs free energies (ΔG eV) of key CO_2RR intermediates on different Cu/PVP surface models.

3 SI-3 References

1 SI-1 Experimental section

1.1 Materials

All chemicals for ink and electrolyte preparation were analytical grade and used without additional purification, and the GDL was used directly as supplied. The following chemicals were used: Copper (II) acetate monohydrate (≥98%, Alfa Aesar), Potassium hydroxide (BioXtra ≥98%, pellets anhydrous, Sigma-Aldrich), Polyvinylpyrrolidone (PVP, K90, AppliChem-Panreac). Absolute ethanol was purchased from Merck, and 2-propanol (Technical, VWR Chemicals). Nafion solution (5 wt%). Ultrapure deionized water was used to prepare solutions. High-purity CO_2, Ar, and H_2 (99.999%, Linde) were used in the study. Nickel foam was used as the counter electrode, and a Nafion 117 as a membrane.

1.2 Electrochemical measurements

Electrochemical CO_2 reduction experiments were performed using a Biologic SP-300 potentiostat in a two-compartment cell separated by a Nafion 117 membrane. A three-electrode arrangement was utilized for electrochemical studies, featuring a platinum sheet as the counter electrode and an Hg/HgO reference electrode. For CO_2 measurements, the device had a dual-compartment configuration, with nickel foam as the anode and a gas diffusion electrode (GDE) as the cathode. The electrolyte, 1 M KOH, was circulated through the electrochemical cell using peristaltic pumps (BT 100 M) at a flow rate of 1 mL min^{-1}. A mass flow controller regulated the CO_2 flow at 20 mL min^{-1}. Chronopotentiometry (CP) was employed for all CO_2 measurements using freshly prepared GDE. Linear sweep voltammetry (LSV) tests were conducted at a scan rate of 10 mV s^{-1} over the potential range from 0 to -0.9 V *versus* RHE. All recorded potentials were converted into the reversible hydrogen electrode (RHE) scale using the formula: $E_{RHE} = E_{Hg/HgO} + 0.098\ V + 0.0591 \times pH$. Cyclic voltammetry (CV) tests at different scan rates from 10 to 120 mV s^{-1} were performed to determine the electrochemical active surface area (ECSA) under a potential window where no Faraday reaction, and then the geometric double layer capacitance (Cdl) was determined by calculating the current density difference $\Delta J = (J_{anodic} - J_{cathodic})/2$ as a linear correlation with the scan rate at a given potential. Furthermore, the EIS measurement was performed at the operating voltage, with a frequency range of 100 kHz to 10 mHz. Following impedance measurements, the Distribution of Relaxation Times (DRT) analysis was employed to better understand the fundamental electrochemical processes by separating them over several time frames.

1.3 Material Characterization.

X-ray diffraction (XRD) patterns were recorded on a Rigaku MiniFlex 600 diffractometer in the 2θ range of 10°–80° with a step size of 0.007°. X-ray photoelectron spectroscopy (XPS) was performed on a Kratos Axis Ultra instrument, with all spectra internally calibrated using the C 1s peak at 284.7 eV. Surface morphology was analyzed via scanning electron microscopy (SEM) using a TESCAN VEGA COMPACT with a tungsten filament. Elemental analysis was performed using energy-dispersive X-ray spectroscopy (EDS) on a JEOL Neoscope JCM-6000 Plus benchtop SEM. Atomic force microscopy (AFM) measurements were obtained using a Veeco Dimension 3100 instrument to assess surface topography at the nanoscale. Structural analysis was carried out using transmission electron microscopy (TEM).

1.4 Double-Layer Capacitance (Cdl) from CV and EIS

The electrochemical double-layer capacitance (C_{dl}) of the materials was estimated from cyclic voltammetry (CV) at different scan rates, which were performed to determine the electrochemically active surface area (ECSA) within a limited potential range without any faradaic processes (-0.05 to -0.15 V vs. Hg/HgO). Then, the geometric double-layer capacitance (C_{dl}) was determined by calculating the current density difference ΔJ = (J anodic – J cathodic)/2 as a linear function of the scan rate at a given potential.

The ECSA was calculated using the following**: Equation S1.**

$$ECSA = \frac{C_{dI}}{C_s} \times ASA \qquad 1$$

Here, $\mathbf{C_{dl}}$ is the specific capacitance of the sample, and **ASA** is the actual electrode surface area. $\mathbf{C_S}$ is 40 mF/cm2, representing the standard theoretical capacitance of the electrode's complete flat surface.

Electrochemical impedance spectroscopy (EIS) can be used to determine a double-layer capacitance value, which can be extrapolated from the Constant Phase Elements (CPE) using **Equation S2**.

$$C_{CPE} = [Q(R_e^{-1} + R_{CT}^{-1})^{(\alpha - 1)}]^{\frac{1}{\alpha}} \qquad 2$$

2 SI-2 Figures and Tables

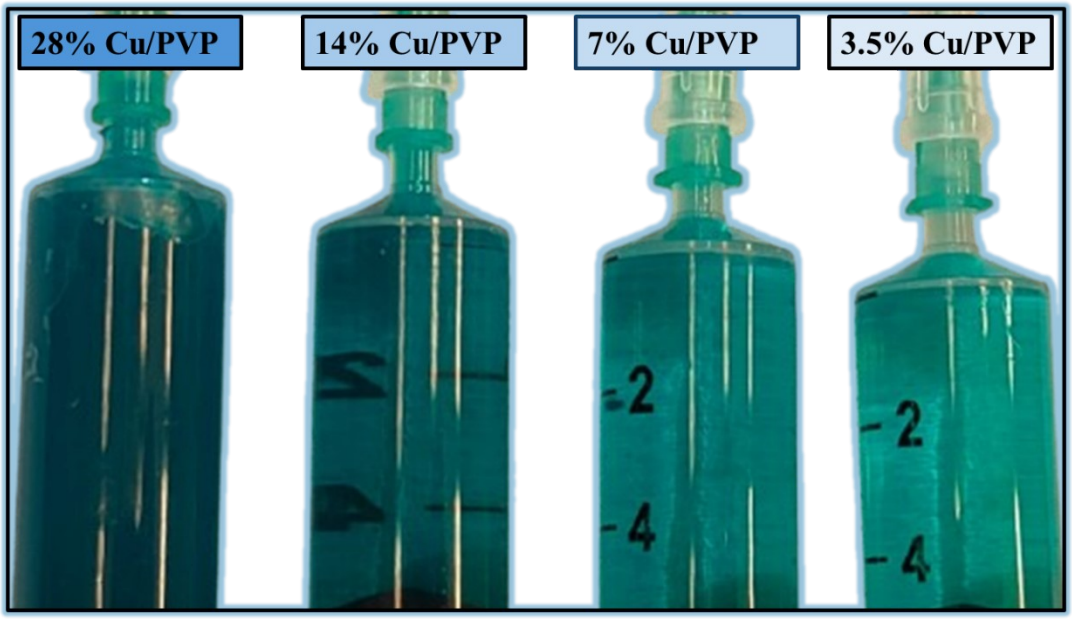

Figure S1. Photographs of the four precursor syringes containing Cu acetate/PVP solutions at different Cu loadings (3.5%, 7%, 14%, and 28%).

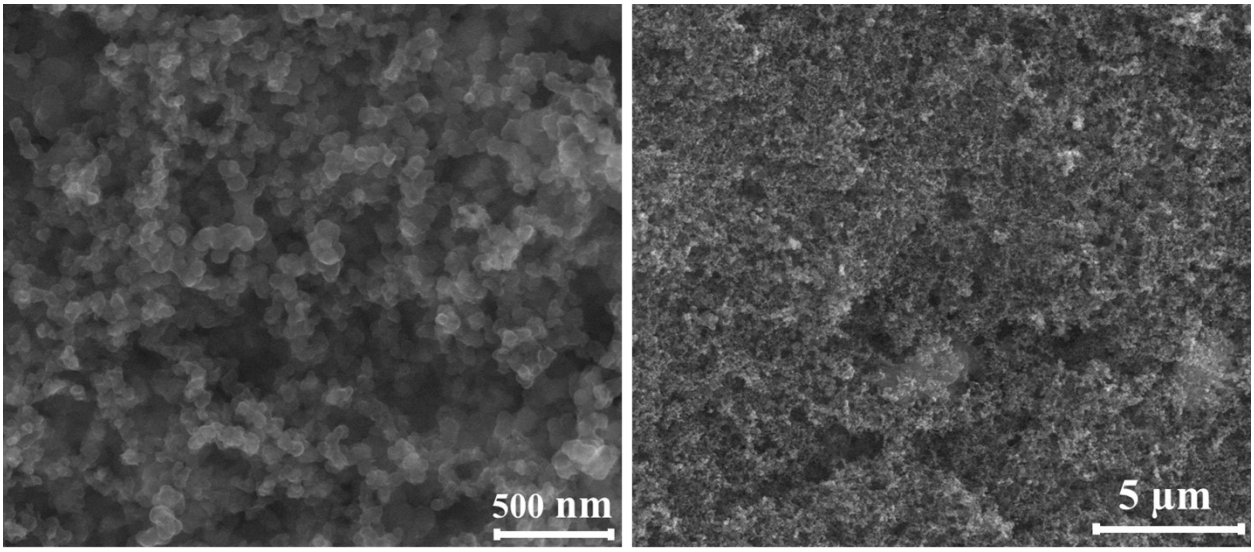

Figure S2. SEM images of the gas diffusion layer (GDL) before catalyst deposition.

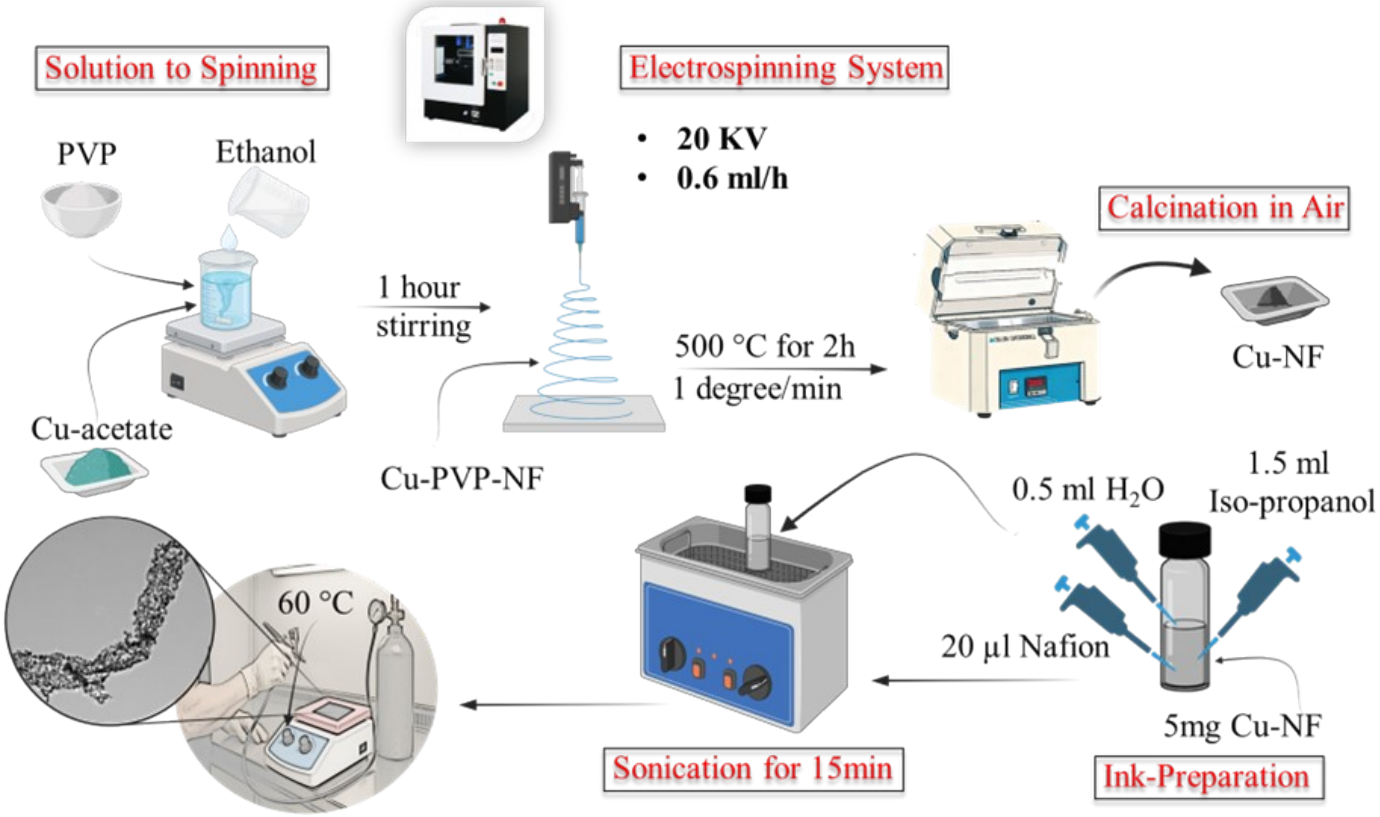

Figure S3. Schematic of Cu-nanofiber GDE fabrication: solution preparation, electrospinning, calcination to Cu NFs, ink preparation, and GDE fabrication.

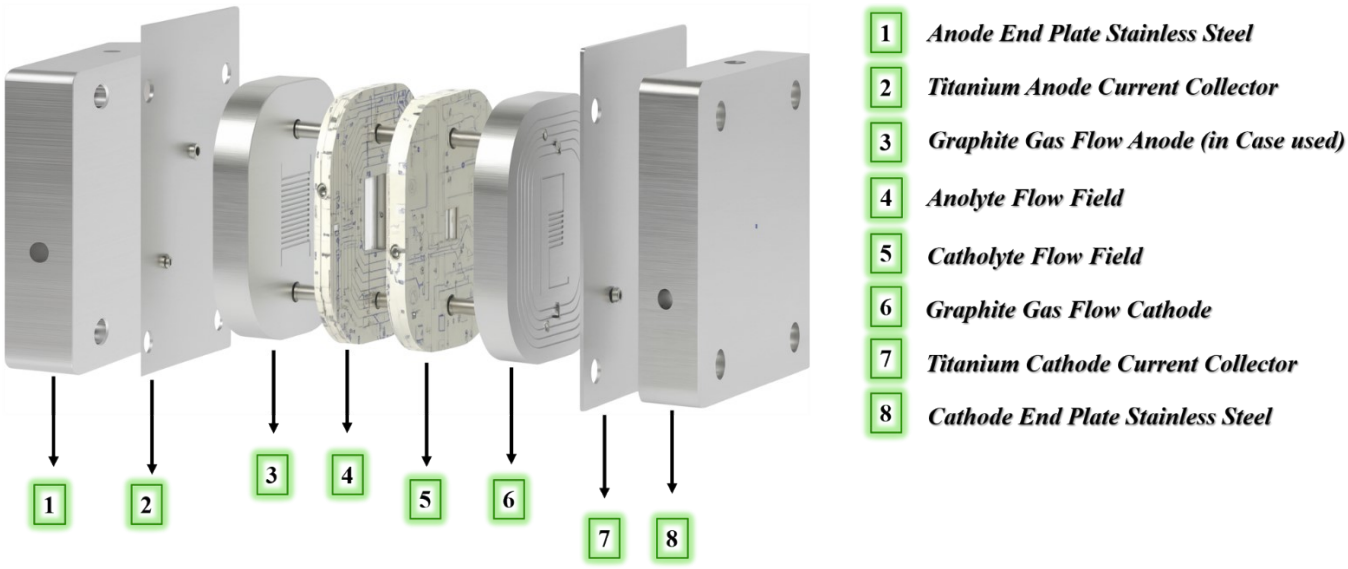

Figure S4. Schematic illustration of the flow electrolyzer cell.

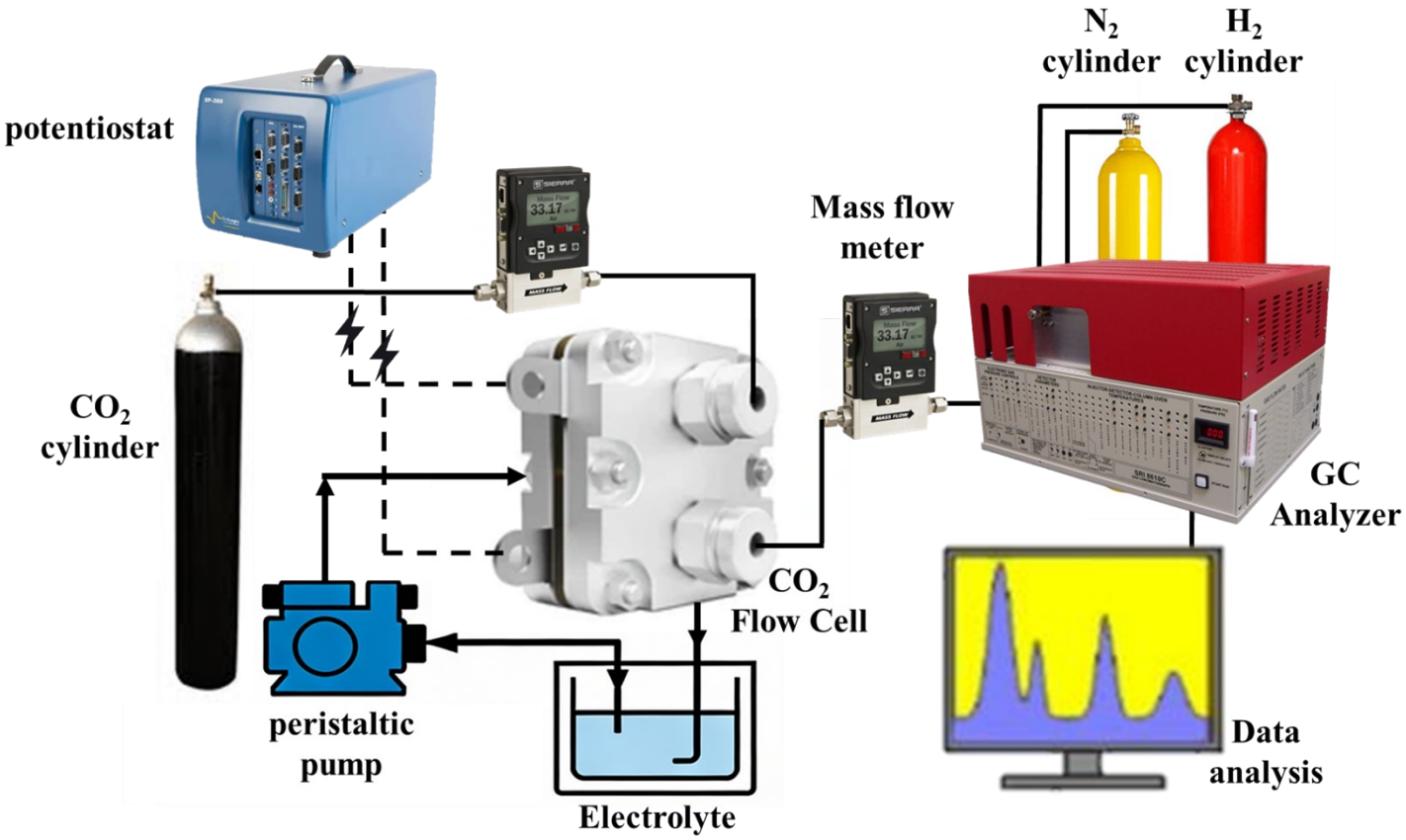

Figure S5. Image of the experimental setup for the electrochemical CO_2 reduction reaction (CO_2RR).

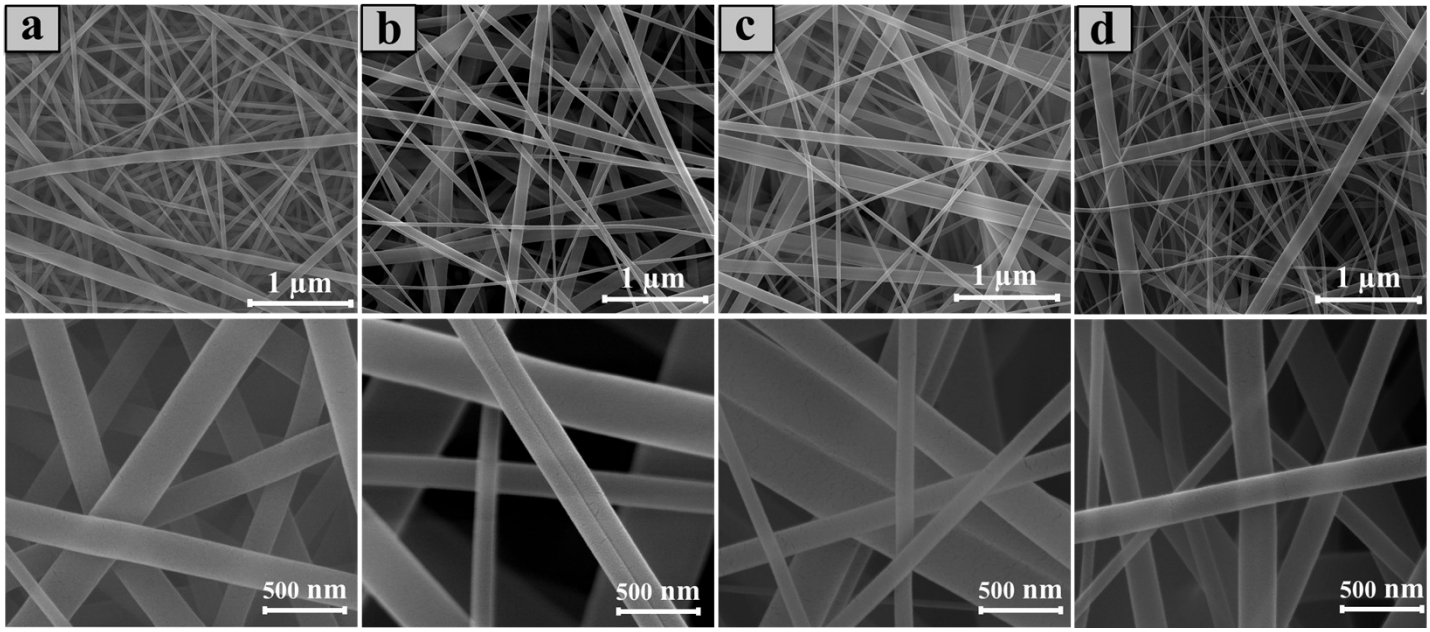

Figure S6. SEM pictures of Cu/PVP nanofibers at Cu concentrations of (a) 3.5%, (b) 7%, (c) 14%, and (d) 28%. The top row (1 μm): entire fiber morphology and network structure. Bottom row (500 nm).

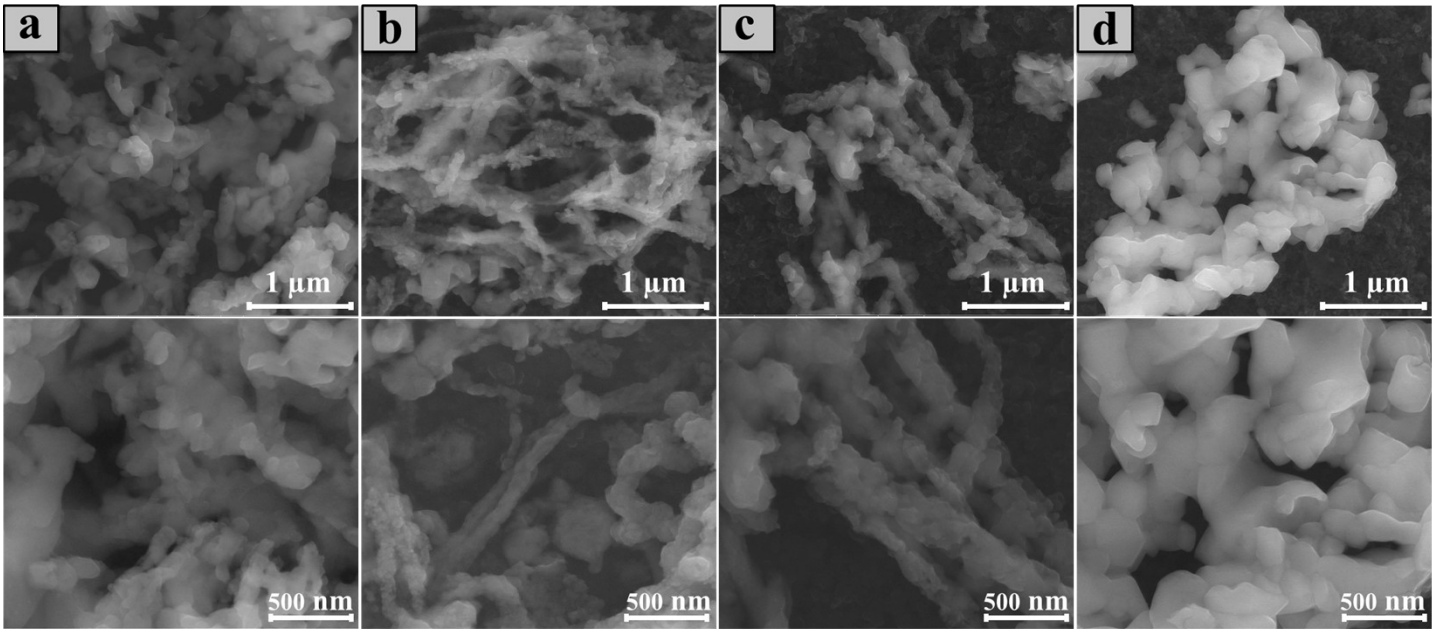

Figure S7. SEM pictures of calcined Cu/PVP samples on the GDL (a) 3.5%, (b) 7%, (c) 14%, and (d) 28%. Top row (1 μm): comprehensive morphology of the calcined structures on the gas diffusion layer (GDL); Bottom row (500 nm).

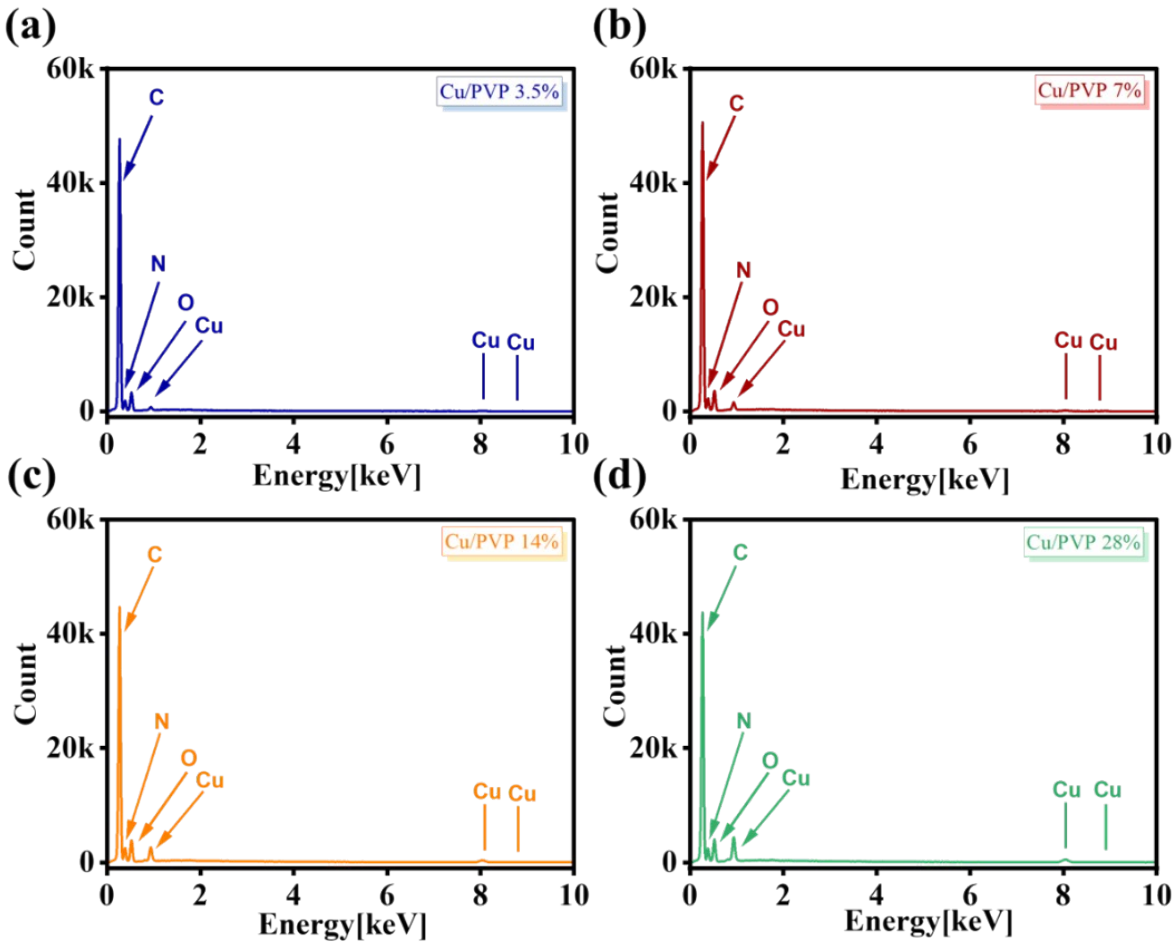

Figure S8. EDX measurements of all Cu/PVP fibers before calcination. (a) Cu/PVP 3.5%, (b) Cu/PVP 7%, (c) Cu/PVP 14%, (d) Cu/PVP 28%.

Table S1. Elemental composition of all Cu/PVP fibers before calcination, as revealed from the EDX analysis.

Element	Cu/PVP 3.5%	Cu/PVP 7%	Cu/PVP 14%	Cu/PVP 28%
Sample	Mass%			
Cu	0.78	1.85	4.64	6.76
C	92.12	90.79	86.90	85.05
N	4.23	4.43	4.96	4.73
O	2.87	2.93	3.50	3.46

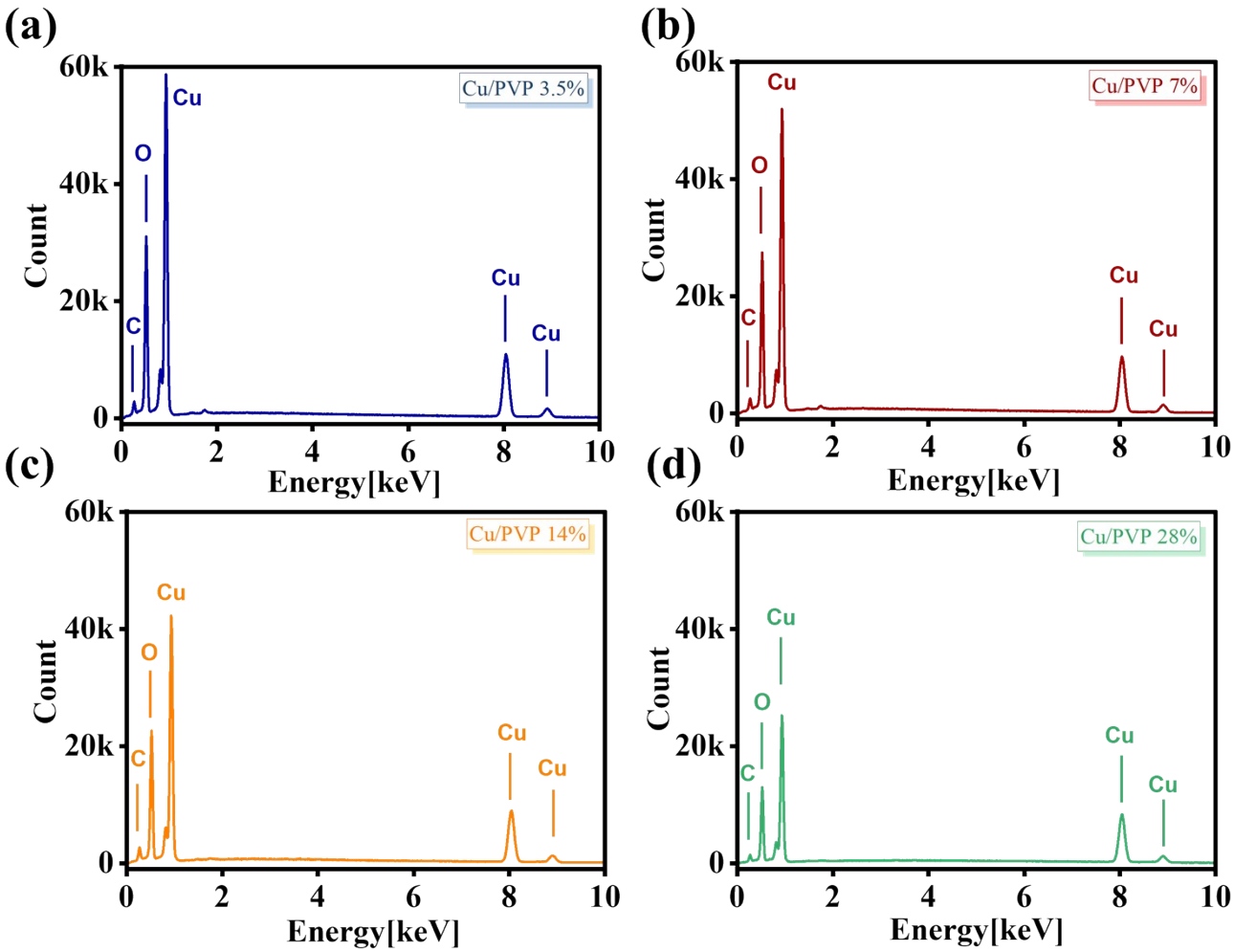

Figure S9. EDX measurements of all Cu/PVP powder after calcination. (a) Cu/PVP 3.5%, (b) Cu/PVP 7%, (c) Cu/PVP 14%, (d) Cu/PVP 28%.

Table S2. Elemental composition of all Cu/PVP powder after calcination, as revealed from the EDX analysis.

Element	Cu/PVP 3.5%	Cu/PVP 7%	Cu/PVP 14%	Cu/PVP 28%
Sample	Mass%			
Cu	82.1	81.49	82.72	88.76
C	2.23	2.53	3.23	1.96
O	15.67	15.53	14.04	9.28

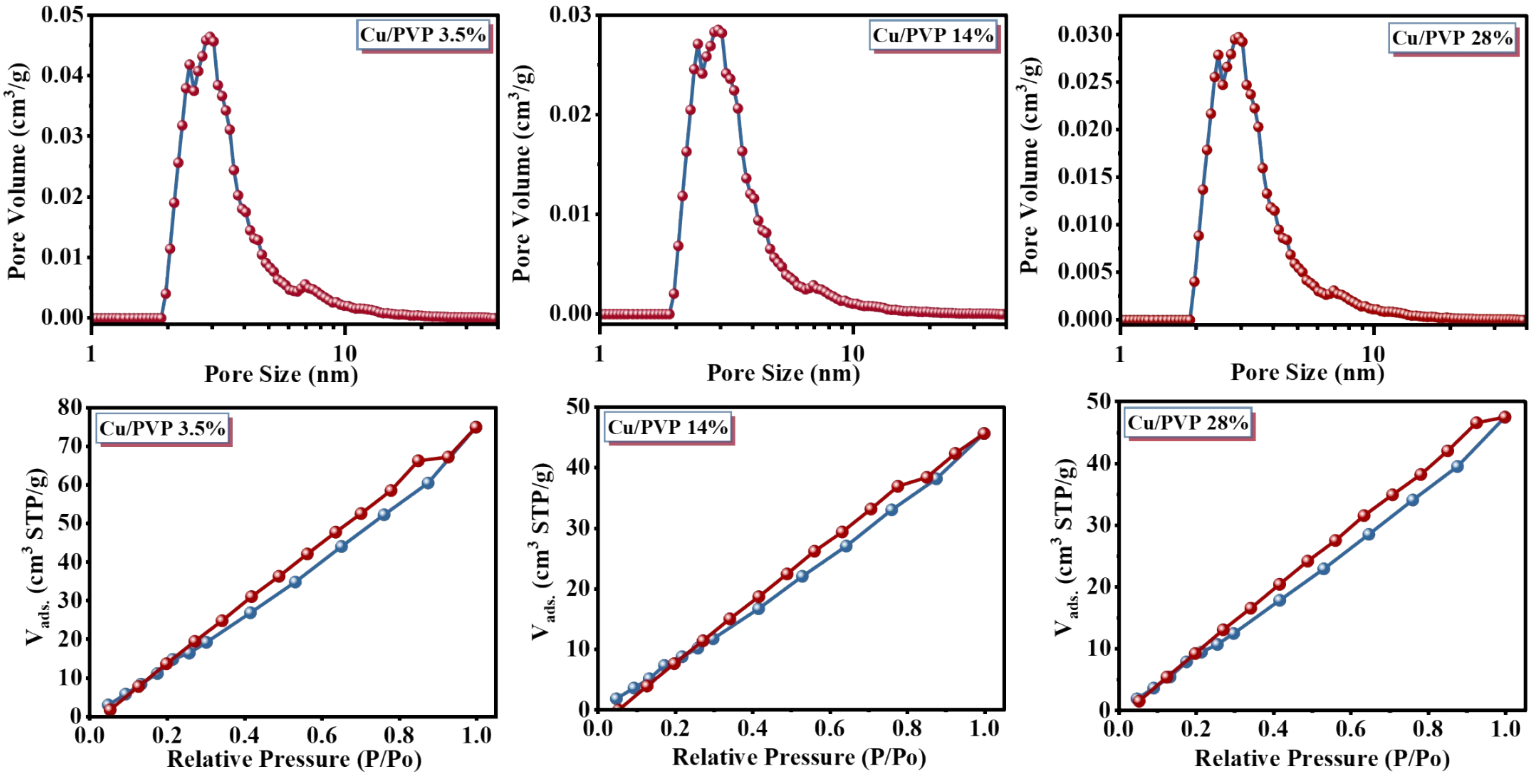

Figure S10. The N_2 adsorption/desorption isotherms and BJH pore size distribution for Cu/PVP 3.5%, 14%, and 28%.

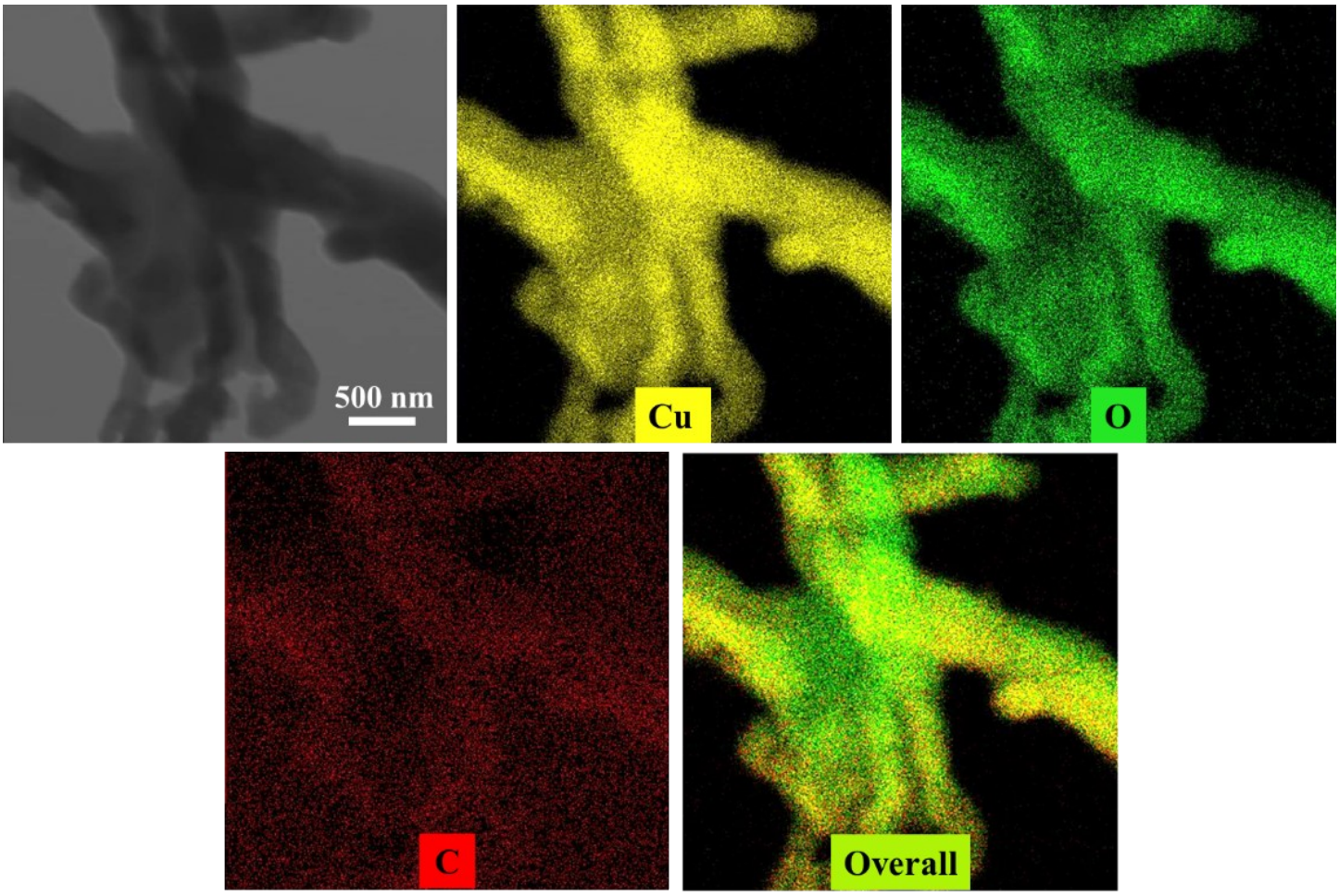

Figure S11. TEM image and corresponding EDS elemental mapping of the Cu/PVP 28% composite.

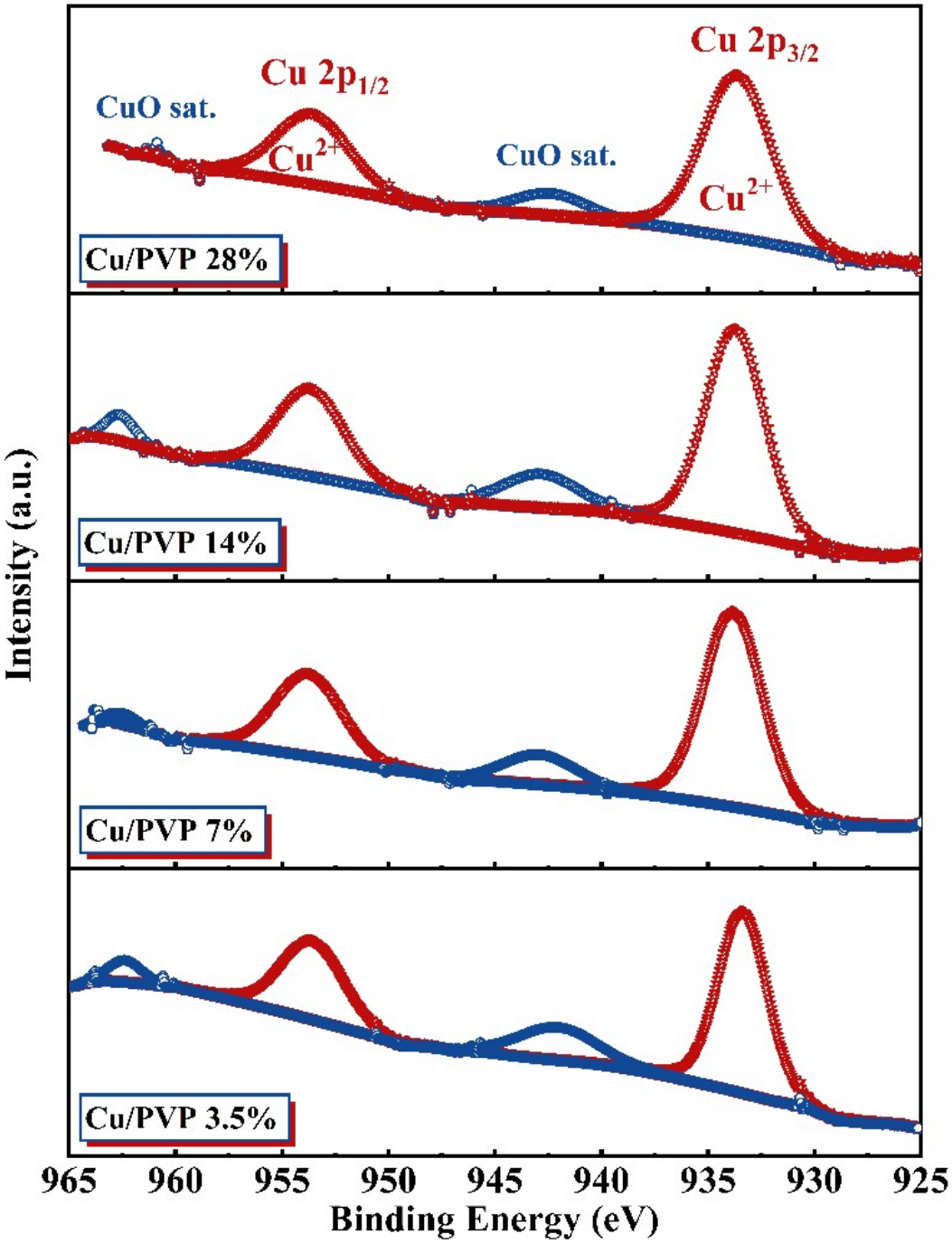

Figure S12: XPS of the Cu 2p for all Cu/PVP nanofiber samples.

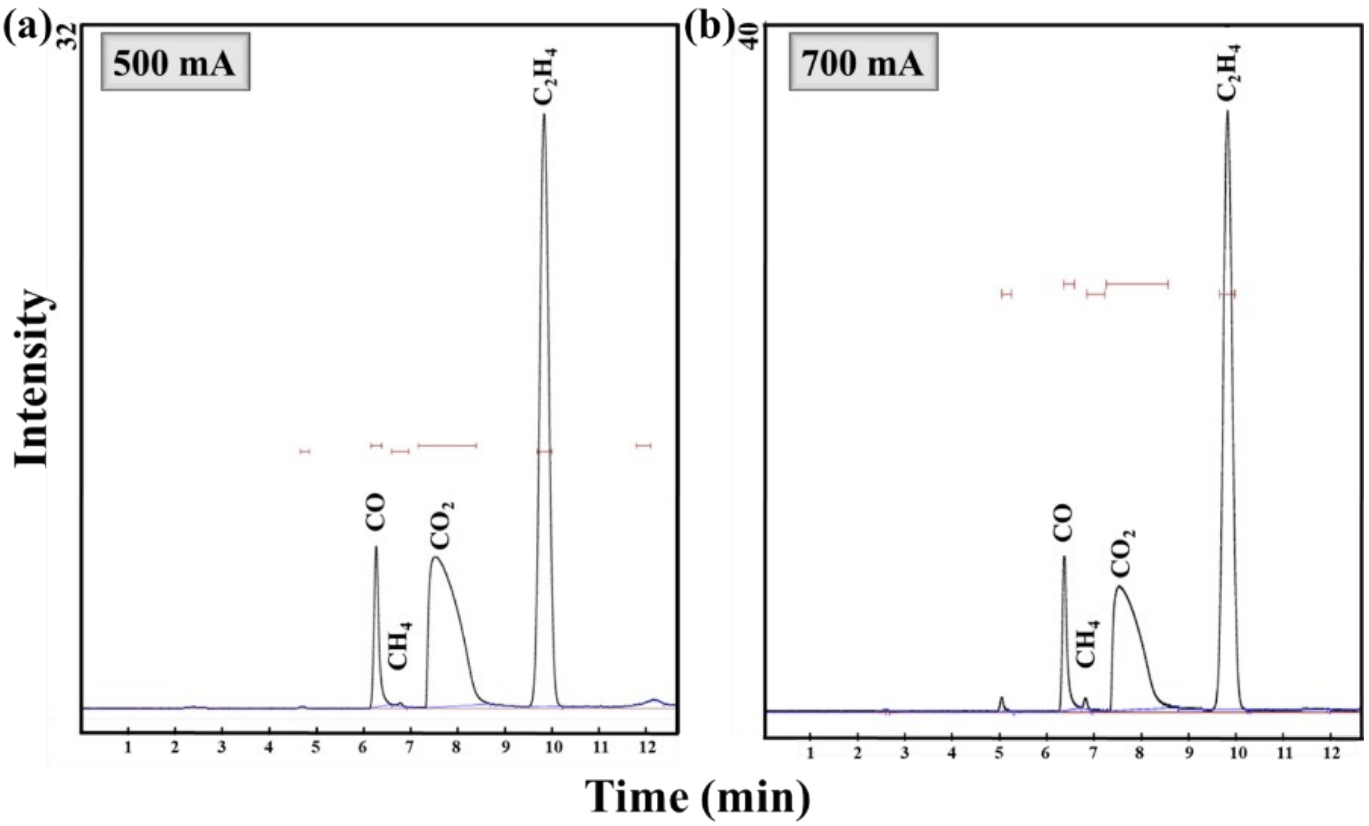

Figure S13: GC spectra of Cu/PVP 7% (a) at 500 mA/cm^2 (b) at 700 mA/cm^2

Table S3. Comparison of the FE of ethylene with the most relevant literature.

Material	Electrolyte	Cell Type	Potential vs. RHE	FE% of C_2H_4	C_2H_4 current density	Reference
Th-TF COF modified Cu_3N catalyst.	0.5 M K_2SO_4 + H_2SO_4 (Anode)	AEM (Zero-gap MEA)	~4.5V	~50%	311 mA cm^{-2}	[1]
CuZnO-PVP	0.3 M KI + 0.1 M $KHCO_3$	H-cell	−1.0 V	50.2 %	10 mA cm^{-2}	[2]
Cu/PTFE (M_Cu, hydroxylated)	0.1 M $KHCO_3$	Flow cell	−0.25V	55.1%	55 mA cm^{-2}	[3]
m-SiO_2/CuO	1 M KOH	Flow cell	N/A	55.5 %	333 mA cm^{-2}	[4]
Dual-Phase Cu	3 M KCl	Flow cell	N/A	81 % C_2 products	322 mA cm^{-2}	[5]
TA Cu	1 M KOH	Flow cell	−1.2 V	63.6 %	316 mA cm^{-2}	[6]
OD-Cu-800	1 M $KHCO_3$	Flow cell	−0.94 V	81.5% C_2 products	285 mA cm^{-2}	[7]
Cu_2O microcrystals	0.1 M $KHCO_3$	H-cell	−1.38V	42.0%	7.1 mA cm^{-2}	[8]
Cu_2O–Zn-5%	1 M KOH	Flow cell	−1.1 V	~52 %	~177 mA cm^{-2}	[9]
Nanoporous Cu	1 M KOH	Flow cell	−0.67 V	38.6 %	252 mA cm^{-2}	[10]
Cu_1Ni-BDP MOF	1 M KOH	Flow cell	-1.3 V	52.7%	278 mA cm^{-2}	[11]
De- Au_1Cu SAA	1 M KOH	Flow cell	-1.1 V	52%	252 mA cm^{-2}	[12]
Cu/PVP 7% Porous NFs	**1 M KOH**	**Flow cell**	**- 0.76 V**	**56±4%**	**330 mA cm^{-2}**	**This Work**

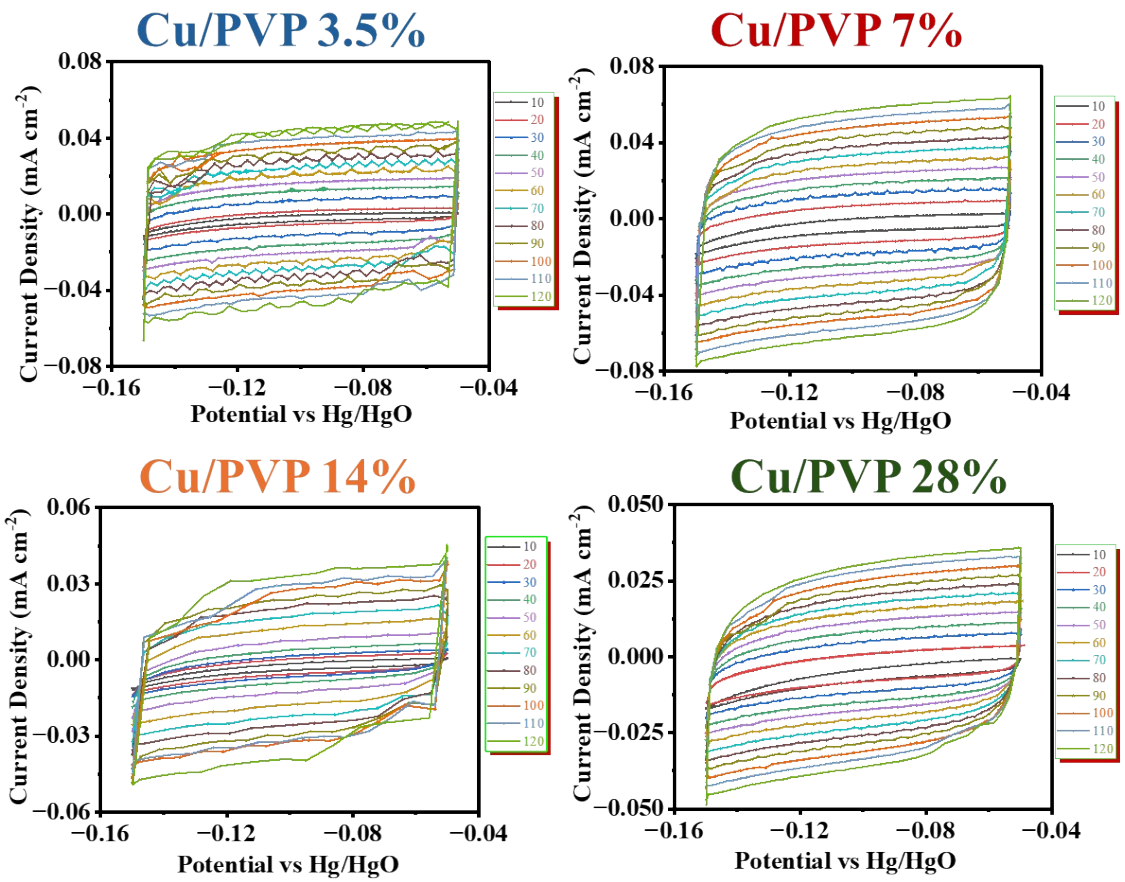

Figure S14. ECSA measurements of the Cu/PVP samples. (a, b, c, d), Cyclic voltammetry profiles were obtained for the 3.5%, 7%,14% and 28% samples at sweep rates of 10, 20, 30, 40, 50, 60, 70, 80, 90, 100, 110, and 120 mV/s, respectively.

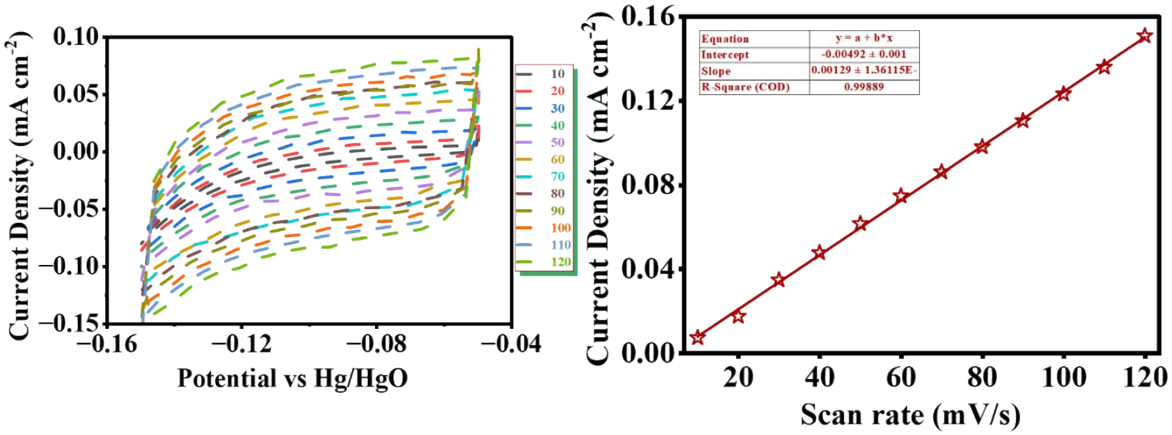

Figure S15. CV at different scan rates and ECSA measurements of the Cu/PVP 7% after short-term CO_2RR operation.

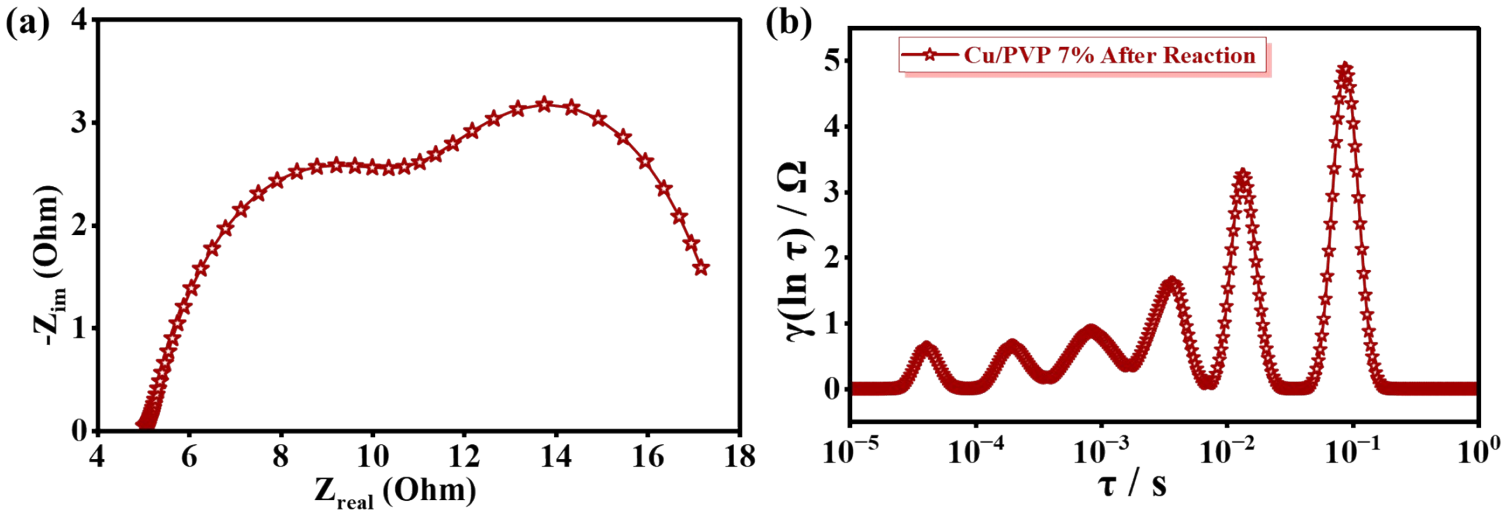

Figure S16. **(a)** Nyquist plots obtained from EIS measurements. **(b)** Distribution of relaxation times (DRT) spectra of the Cu/PVP 7% after short-term CO_2RR operation.

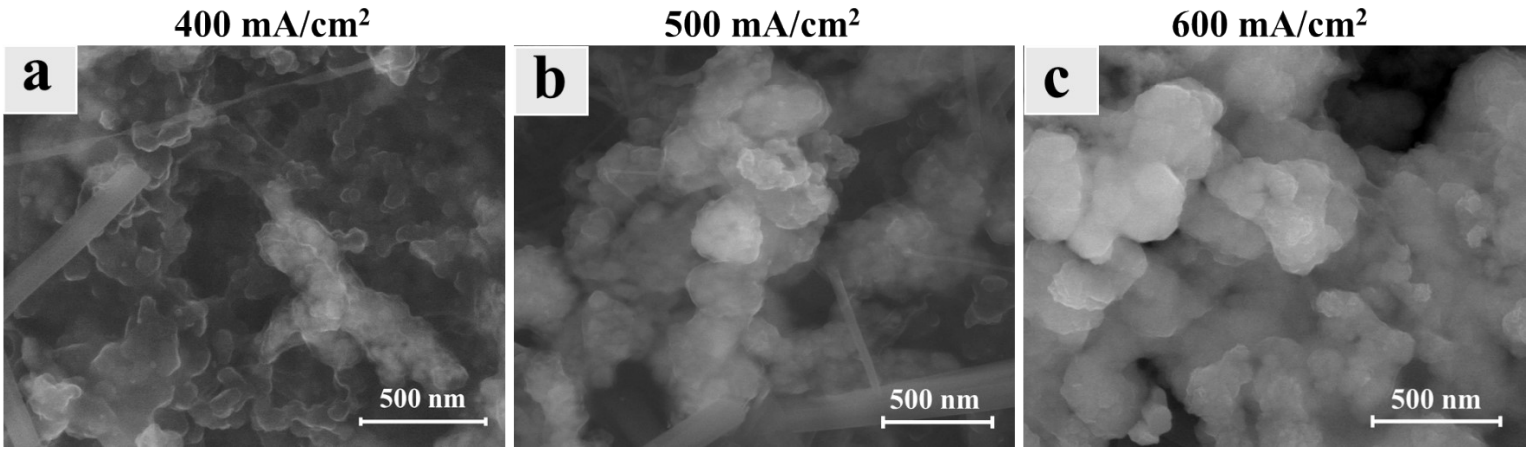

Figure S17. SEM images of Cu/PVP 7% after stability measurement at current densities of **(a)** 400 mA, **(b)** 500 mA, and **(c)** 600 mA.

Table S4. Calculated Gibbs free energies (ΔG eV) of key CO_2RR intermediates on different Cu/PVP surface models.

Intermediate	Cu/PVP 3.5% (eV)	Cu/PVP 7% (eV)	Cu/PVP 14% (eV)	Cu/PVP 28% (eV)
*CO	0.13	0.02	0.29	0.31
*COH	1.52	1.12	1.88	2.11
*OCCOH	1.96	1.35	2.33	2.81
*OH_2C_2H	-0.31	-0.45	-0.08	0.18

The Cu/PVP 7% model exhibits relatively more favorable energetics for key CO_2RR intermediates compared with the other surface models, suggesting enhanced interaction with carbon-containing intermediates on the roughened Cu surface.

3 SI-3 References

1. D. Chen, J. Liu, Y. Yuan, X. Han, K. Zhang, Q. Hu, S. Han, S. Xi, Q.-H. Yang and K. P. Loh, *Nature Communications*, 2025, **16**, 10783.
2. L. Zhou, H. W. Tsai, T. W. Kuo, J. C. Kao, Y. C. Lo, J. M. Chang, T. H. Chiang, S. Dai, K. W. Wang and T. Y. Chen, *Advanced Science*, 2025, 2501642.
3. Y. Wang, H. Huang, S. Zhang, H. Zhang, C. Jing, J.-Q. Wang and L. Zhang, *Chemical Communications*, 2024, **60**, 12710-12713.
4. J. Zhu, S. Wang, J. Zhang, Z. Fang, W. Ji, G. Lin, L. Guo, B. Li, J. Wang and J. Fu, *Chemical Engineering Journal*, 2024, **494**, 153189.
5. P.-P. Yang, X.-L. Zhang, P. Liu, D. J. Kelly, Z.-Z. Niu, Y. Kong, L. Shi, Y.-R. Zheng, M.-H. Fan and H.-J. Wang, *Journal of the American Chemical Society*, 2023, **145**, 8714-8725.
6. S. Chen, C. Ye, Z. Wang, P. Li, W. Jiang, Z. Zhuang, J. Zhu, X. Zheng, S. Zaman and H. Ou, *Angewandte Chemie*, 2023, **135**, e202315621.
7. C. Li, Z. Guo, Z. Liu, T. Zhang, H. Shi, J. Cui, M. Zhu, L. Zhang, H. Li and H. Li, *ACS Catalysis*, 2023, **13**, 16114-16125.
8. W. Dong, D. Fu, Z. Zhang, Z. Wu, H. Zhao and W. Liu, *Frontiers in Chemistry*, 2024, **12**, 1482168.
9. Y. Jia, Y. Ding, T. Song, Y. Xu, Y. Li, L. Duan, F. Li, L. Sun and K. Fan, *Advanced Science*, 2023, **10**, 2303726.
10. J. J. Lv, M. Jouny, W. Luc, W. Zhu, J. J. Zhu and F. Jiao, *Advanced Materials*, 2018, **30**, 1803111.
11. L. Huang, Z. Liu, G. Gao, C. Chen, Y. Xue, J. Zhao, Q. Lei, M. Jin, C. Zhu and Y. Han, *Journal of the American Chemical Society*, 2023, **145**, 26444-26451.
12. Y. Zhao, Y. Wang, Z. Yu, C. Song, J. Wang, H. Huang, L. Meng, M. Liu and L. Liu, *ACS nano*, 2025, **19**, 4505-4514.